Optics Letters

Versatile hybrid plasmonic microfiber knot resonator

Jin-Hong Li,[1] Jin-Hui Chen,[1] Shao-Cheng Yan,[1] Ya-Ping Ruan,[1,2] Fei Xu,[1,*] and Yan-Qing Lu[1]

[1]College of Engineering and Applied Sciences, Nanjing University, Nanjing 210093, China
[2]e-mail: bnuryp@126.com
*Corresponding author: feixu@nju.edu.cn

Received 5 May 2017; revised 8 July 2017; accepted 25 July 2017; posted 27 July 2017 (Doc. ID 295218); published 25 August 2017

A planar, all-optical fiber polarizer-based device based on a hybrid plasmonic microfiber knot resonator (HPMKR) is demonstrated in this Letter. A microfiber knot resonator (MKR) can be flexibly attached to the gold film, which forms the hybrid plasmonic mode with high propagation loss. Therefore, the device can be used not only as a broadband polarizer, but also as a high-quality resonator by tuning the geometry of the MKR. The polarizer has an extinction ratio of more than 15 dB ranging from 1200 to 1600 nm, and the Q-factor is more than 52,000 for one polarization state. For a chosen polarization, the resonator has an extinction ratio of nearly 15 dB, even though the diameter of the microfiber is more than 5 μm, which is unattainable for a normal MKR. By further optimizing and packaging, the device can be utilized as a weight sensor, with a sensitivity of 18.28 pm/g (51.2 pm/kPa) for the cavity resonant wavelength. Further, a vibration sensor on a HPMKR structure for detecting vibration from tens of hertz to several kilohertz is demonstrated.

OCIS codes: (060.2310) Fiber optics; (230.5750) Resonators.

https://doi.org/10.1364/OL.42.003395

Manipulating and controlling the pollarization state of light is of great importance in the sensor, optical communication, and fiber laser system. Compared with the traditional polarization beam splitter [1], fiber-based polarization-controlling components (PCCs) have many advantages: easier alignment, smaller insertion loss, and compatibility with fiber systems. There are some kinds of PCCs available, such as graphene polarizers [2], W-profile fibers [3], hole-assisted fibers [4], but these devices have to be straightly arranged, and the diameter of fiber is more than 100 μm; these critical service conditions often inhibit realistic versatile applications.

Surface plasmon-polaritons (SPPs) [5] are attracting attentions due to their great capacity of field intensity enhancement and light confinement beyond the diffraction limit [6]. However, there is a balance between light confinement and propagation loss for the SPP waveguides [7,8]. One way to address this issue is to explore the hybrid plasmonic waveguide, such as a nanofiber attached to a metal film [9,10], a nanofiber attached to a Bragg grating [11], a waveguide on metallic bump structure [12], and a hybrid metal V-groove [13]. Recently, microfiber-based devices show great potential in fiber-optics applications for their compactness, flexibility, and high sensitivity. The microfiber knot resonator (MKR) is one of the optical microring resonators. The MKR has many advantages such as low insertion loss, high finesse, easy fabrication, and compatibility with fiber systems. It can be utilized as an add–drop filter [14], a current sensor [15], and a magnetic-filed sensor [16], etc. However, most of the reported MKRs are made of cutoff microfiber, with high insertion loss and poor mechanical behavior, which will inhibit the realistic application. In addition, the combination of the SPP and MKR for enhanced sensing applications is hardly reported.

Our previous work demonstrated a stereo structure combining a high-Q resonator and a 3D miniature polarizer [17]. Here, we pave another way to realizing a miniature planar, all-optical fiber single-polarization high-Q resonator. In this Letter, we report a hybrid plasmonic microfiber knot resonator (HPMKR) composed of a MKR situated on a smooth gold film. There is a hybrid plasmonic mode excited by the metal surface SPP mode and the microfiber dielectric mode. The MKR can be flexibly attached on the gold film. We can adjust the device structure easily by tuning the length and angle. Here, with the help of lab-on-a-chip technique [18], we make a polarizer with the extinction ratio of more than 15 dB from 1200 to 1600 nm, and the Q-factor is more than 52,000. The fabrication process permits easy handing and inexpensive. Further, we package the HPMKR with polydimethylsiloxane (PDMS), and a robust device is obtained. In addition, it can be utilized as a weight sensor, an optical switch, and a vibration sensor.

Figure 1 shows the fabrication process of the HPMKR. To avoid the loss introduced by the dust adhering to the glass slide surface, an ultrasonic cleaning procedure was necessarily accomplished beforehand. The glass slide was deposited with a gold film with thickness ~100 nm. The MKR was made of a silica microfiber which was directly drawn from a standard single-mode optical fiber (SMF-28, Corning, U.S.) by the flame brushing method [19,20]. The MKR was fabricated by tying a microfiber by hand with the help of high-precision translation stages [21]; this method ensures a no-cutting and compact MKR

structure made from a double-ended tapered fiber. The MKR was attached to the prepared glass slide (with gold film) by another translation stage. Then a HPMKR was realized. In order to enhance the robustness of devices for practical situations, the HPMKR was embedded in PDMS (sylgard 184 silicone elastomer, Dow Corning). We choose PDMS because it has a low refractive index and high optical transparentness. Besides, it is biocompatible and highly stretchable, and various surface treatments can be employed to modify its hydrophobic surface to fit different applications. The PDMS-sealed HPMKR will combine the feature of both and may be used for some bio-application in the future.

The HPMKR consists of a MKR and a gold film substrate. Due to the lack of circular symmetry, the coupling in the twisting region of a MKR should be polarization dependent. The detailed theoretical model for a MKR is reported in Ref. [22]. In our case, we find that the polarization state in the HPMKR is loosely coupled because of formation of a hybrid plasmonic mode and a short twisting length in the MKR [22]. Therefore, we can simply regard MKR as an optical ring resonator. Since the ring section contacts the metal surface, the coupling between the plasmonic mode supported by gold film and the waveguide modes leads to a hybrid plasmonic modes (transverse-magnetic-like mode) [17] and strong polarization-dependent characteristics. As for a MKR by tying microfiber, the resonant condition can be expressed as in the following:

$$n_{\text{eff}} \times L = m\lambda_{\text{res}}, \tag{1}$$

where n_{eff} is the effective refractive index, L is the MKR length, λ_{res} is the resonant wavelength, and m is an integer.

The theoretical results for the typical transmittance spectra of a HPMKR are shown in Fig. 2(c). The coupling length is ~120 μm, the diameter of the microfiber is ~5 μm, the diameter of the MKR is ~1 mm. the thickness of gold film is 100 nm, the refractive index of gold is $0.5582 + 10.756i$ at 1550 nm, and the refractive index of PDMS is 1.3997 at the wavelength of 1550 nm. The intensity transmittance of the MKR can be obtained as in the following: [23]

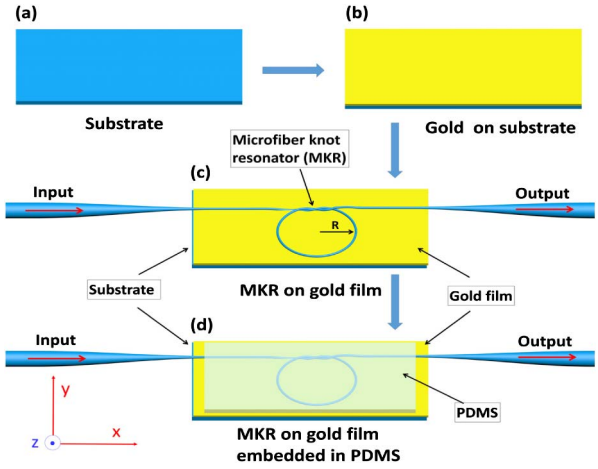

Fig. 1. Fabrication process of a HPMKR. (a) A silica substrate is functionalized by (b) coating ~100 nm gold film, (c) attaching a MKR on the gold film, and (d) embedding the MKR in PDMS.

higher than the LMM. The calculated Q-factor for HMM and LMM are 57,600 and 70,200 respectively. The lower Q-factor for HMM can be attributed to the larger propagation loss and smaller coupling coefficient because of the localization of the hybrid plasmonic mode. The theoretical model fits well with the experimental results, which will be discussed in the next section.

The optical measurement system is shown as Fig. 3(a). Light from an amplified spontaneous emission light source (1525–1565 nm) was linearly polarized by a polarizer, and then a polarization controller (PC) was used to compensate for the birefringence of the circuit. In this way, we can control the input light polarization to selectively excite different optical modes in the HPMKR. The transmission spectrum was recorded by an optical spectrum analyzer (OSA, Yokogawa, AQ6370C). The inset shows the microscope image of a MKR. Figure 3(b) illustrates a MKR lying on a gold film substrate,

$$T = (1-\gamma)\left\{1 - \frac{[1-(1-\gamma)\exp(-\rho L)]\sin^2(\kappa l)}{\left[1-(1-\gamma)^{1/2}\exp\left(-\frac{\rho}{2}L\right)\cos(\kappa l)\right]^2 + 4(1-\gamma)^{1/2}\exp\left(-\frac{\rho}{2}L\right)\cos(\kappa l)\sin^2(\beta L/2)}\right\}, \tag{2}$$

where κ, l, γ, and ρ denote the mode-coupling coefficient of the coupling region, the coupling length, the intensity-insertion-loss coefficient and the intensity attenuation coefficient of the MKR, respectively.

The electric field distributions of both modes are illustrated in Figs. 2(a) and 2(b). For the high-metal-coupling-loss mode (HMM) and low-metal-coupling-loss mode (LMM), they will suffer different loss during the microfiber ring section. In addition, using the finite element method, we can numerically investigate the polarization-related loss mechanism [17], Fig. 2(c) shows the calculated spectrum of the HPMKR for HMM and LMM. Since the HMM suffers higher propagation loss than the LMM, the insertion loss of HMM is naturally

and the SEM image of the MKR is shown in Fig. 3(c). In this Letter, the diameter of the microfiber we use is ~5 μm, and the diameter (0.5–3 mm) of the MKR is adjusted for purpose.

The transmittance spectrum of a bare MKR without gold substrate is shown in Fig. 4(a). The insertion loss is about 1 dB, while the extinction ratio of the spectrum is also negligible (~1 dB). However, when the MKR touches the gold film and forms the HPMKR, the output spectrum is greatly changed, as illustrated in Fig. 4(a). For LMM and HMM modes, they have nearly the same free spectral range (FSR) of 0.216 nm, which is exactly matching the calculated results referring to FSR $= \lambda^2/(n_{\text{eff}}L)$, where λ, n_{eff}, and L are the propagation light wavelength, the effective index of the microfiber, and the single

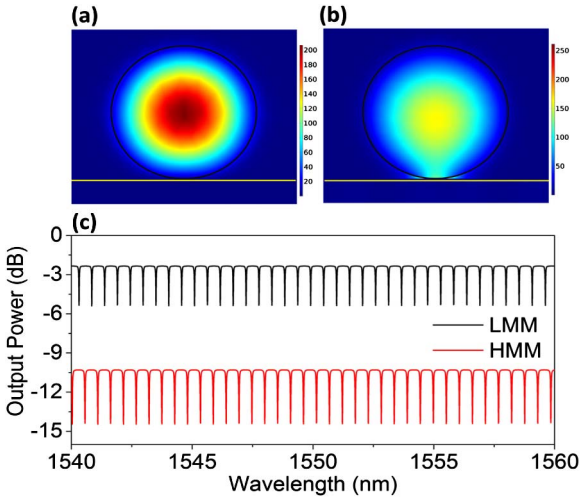

Fig. 2. Cross section and filed distribution of the HPMKR for (a) LMM and (b) HMM. (c) Calculated transmittance spectra for LMM and HMM.

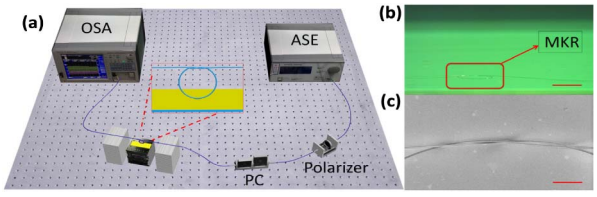

Fig. 3. (a) Optical measurement system. The inset shows a schematic illustration of a MKR on the gold film. (b) MKR lies down on the gold film. The scale bar is 1 mm. (c) SEM image of the MKR coupling area. The scale bar is 50 μm.

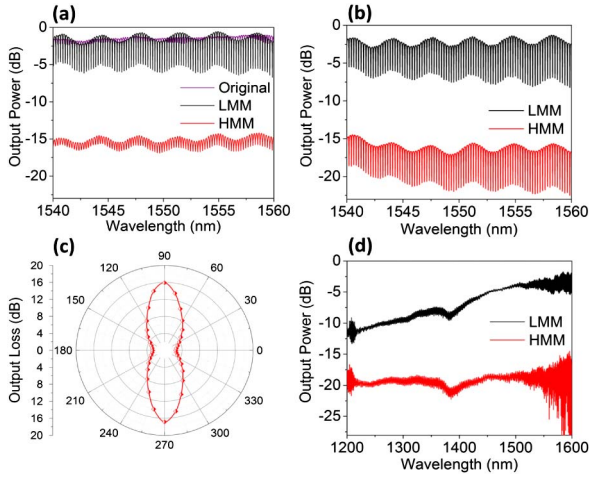

Fig. 4. (a) Transmission spectrum of the HPMKR for two orthogonal modes at 1540–1560 nm. (b) Transmission spectrum at 1540–1560 nm after sealing the HPMKR in PDMS. (c) Output loss as a function of θ at wavelength of 1550 nm for the HPMKR. (d) Broadband polarization of the HPMKR for two orthogonal modes at wavelengths of 1200–1600 nm.

roundtrip length in the resonator, respectively. The extinction ratio for LMM is enlarged, while the insertion loss is almost unchanged, which is probably due to the enhanced coupling induced by the substrate. As for HMM mode, the insertion loss is increased with a slightly enhanced extinction ratio (~2 dB).

Intuitively, the increased loss is caused by the hybrid plasmonic mode for HMM. We find that the measured spectra match well with the theoretical results in Fig. 2(c), and the Q-factor of the HPMKR is more than 52,000. Then, we used PDMS to seal the HPMKR, and the FSR is 0.218 nm, which is possibly caused by the deformation of the MKR structure during the encapsulation procedure. The insertion loss for LMM and HMM is slightly increased. Interestingly, the extinction ratio for both modes is also enhanced, which may be caused by the higher index surroundings. The polar image for the HPMKR is illustrated in Fig. 4(c), which unambiguously indicates that the insertion loss for the HPMKR is highly polarization dependent. Figure 4(d) exhibits the broadband polarization spectrum of the HPMKR, ranging from 1200 to 1600 nm. In addition, we can see that there is a dip near 1380 nm in the spectrum, which is mostly caused by the remaining OH groups released during hydrogen flame heating [24], as we find that the extinction ratio between the LMM and HMM is more than 15 dB.

The weight response characteristics of the aforementioned HPMKR are investigated by loading and unloading the weights on the device. The measured HPMKR was encapsulated in a thin-layer PDMS. The PDMS layer not only enhances the adhesion of the MKR to the gold substrate, but also prevents the MKR from contaminations. The adhesion property between PDMS and glass slide is pretty good. Moreover, for a MKR embedded in PDMS, the temperature-dependent wavelength shift can be suppressed at a certain microfiber diameter because of the opposite thermo-optic effects of optical silica fiber and PDMS [25]. For a MKR made of a 5 μm diameter microfiber, the shift can be less than 5 pm/°C, which is smaller than a typical silica ring resonator of 12–20 pm/°C [25], In our experiment, the environmental temperature change is less than 2°C; even the total shift cannot be read out by an OSA (resolution 0.02 nm), so the device shows good temperature stability during the measurement. For the weight sensor measurement system, we traced the evolution of the optical spectrum of the HPMKR as the weight loading onto the device. Due to the MKR structure, there are periodic wavelength dips in the transmission spectrum corresponding to the resonant wavelength of the HPMKR. We chose a resonant wavelength near 1550 nm to analyze for convenience.

From Fig. 5(a), we can see that the resonant wavelength has an obvious redshift when we increase the loaded weight from 0 to 45 g. The contact area between the loaded weight and our device is 4 mm × 7 mm. The linear response between the resonant wavelength and the loaded weight is depicted in Fig. 5(b). The results of loading and unloading weights keep good linearity and match well with each other. These data correspond to a weight sensitivity of ~18.3 pm/g (51.2 pm/kPa) which is higher than most of the reported optical fiber weight sensors, such as interferometer-based sensors [26] and fiber Bragg grating (FBG)-based sensors [27]. The resonant wavelength shift is mostly caused by the change of polarization and the photoelasticity of PDMS [28].

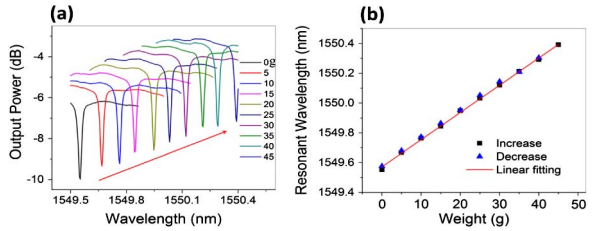

Fig. 5. (a) Transmission spectra of the HPMKR loading a certain weight and (b) the resonant wavelength changing following the different weights.

The resonant wavelength shift will naturally induce the output light power change for a certain light wavelength. As a result, we can use a narrow-band laser (Santec, TSL-710) as a light source and monitor the power change for sensing applications. Figure 6(a) illustrates the output power change relating to the loaded weight. There is a linear dependence between the output power and the loaded weight over a short range. The red line is the linear fitting of the experimental results, which gives a weight sensitivity of 64.21 μW/g. We also measure the ON/OFF response of the device by loading and unloading only 1 g weight, as shown in Fig. 6(b). The cycling measurement results indicate that the HPMKR can perform a fast and stable weigh sensor.

After investigating the static weight response characteristics, we take one step further by testing the HPMKR's dynamic response. Figure 7(a) depicts the vibration measurement

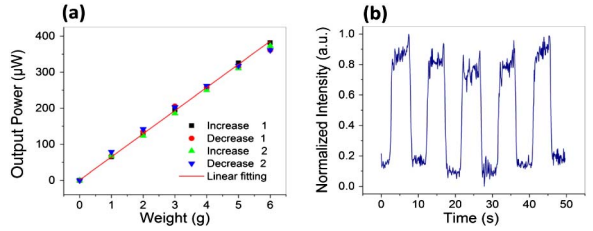

Fig. 6. (a) Output power changes with the weight. The values of the output power have subtracted the starting value. (a) One gram controlled ON/OFF optical switch.

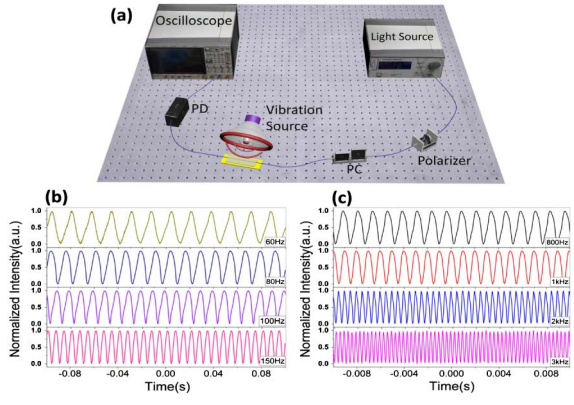

Fig. 7. (a) Vibration sensor measurement system. (b) Response to 60, 80, 100, and 150 Hz. (c) Response to 800, 1000, 2000, and 3000 Hz.

system. The HPMKR was adhered to a vibration source which is controlled by a computer. The output light was detected by a photo-detector, and the transformed electric signal was analyzed by an oscilloscope (Agilent, DSO-X 4024A). Figures 7(b) and 7(c) show that our device has a good vibration response with a frequency range of 60–3000 Hz.

In summary, we have proposed a versatile HPMKR and its sensor applications. By functionalizing the substrate surface with a nanoscale gold film and tuning the structure of the MKR, the HPMKR demonstrates an extinction ratio of more than 15 dB in broadband as a polarizer and a Q-factor of more than 52,000 at the same time. We also fabricated a robust multifunctional sensor by packaging the HPMKR with PDMS. For the weight sensing, it shows 18.28 pm/g (51.2 pm/kPa) for the resonant wavelength. By monitoring the output power change, we show a sensitivity as large as 64.214 μW/g for the output power. We believe this hybrid platform may find applications in optical communication and flexible sensing areas.

Funding. National Natural Science Foundation of China (NSFC) (61475069, 61535005).

REFERENCES

1. J. Chee, S. Zhu, and G. Q. Lo, Opt. Express **20**, 25345 (2012).
2. Q. Bao, H. Zhang, B. Wang, Z. Ni, C. H. Y. X. Lim, Y. Wang, D. Y. Tang, and K. P. Loh, Nat. Photonics **5**, 411 (2011).
3. J. Simpson, R. Stolen, F. Sears, W. Pleibel, J. MacChesney, and R. Howard, J. Lightwave Technol. **1**, 370 (1983).
4. D. A. Nolan, G. E. Berkey, M.-J. Li, X. Chen, W. A. Wood, and L. A. Zenteno, Opt. Lett. **29**, 1855 (2004).
5. R. F. Oulton, V. J. Sorger, D. A. Genov, D. F. P. Pile, and X. Zhang, Nat. Photonics **2**, 496 (2008).
6. W. L. Barnes, A. Dereux, and T. W. Ebbesen, Nature **424**, 824 (2003).
7. Y. Wang, Y. Ma, X. Guo, and L. Tong, Opt. Express **20**, 19006 (2012).
8. Y. Song, J. Wang, Q. Li, M. Yan, and M. Qiu, Opt. Express **18**, 13173 (2010).
9. S. Liu, L. Zhou, H. Wang, and J. Chen, Opt. Express **23**, 16984 (2015).
10. Y. Ma, G. Farrell, Y. Semenova, B. Li, J. Yuan, X. Sang, B. Yan, C. Yu, T. Guo, and Q. Wu, Opt. Laser Technol. **78**, 101 (2016).
11. S. Liu, L. Zhou, J. Xu, X. Wang, and J. Chen, Opt. Express **24**, 9316 (2016).
12. O. Babak and K. Habib, J. Phys. D **47**, 105105 (2014).
13. Z. X. Chen, Z. J. Wu, Y. Ming, X. J. Zhang, and Y. Q. Lu, AIP Adv. **4**, 017103 (2014).
14. X. Jiang, Y. Chen, G. Vienne, and L. Tong, Opt. Lett. **32**, 1710 (2007).
15. K. S. Lim, S. W. Harun, S. S. A. Damanhuri, A. A. Jasim, C. K. Tio, and H. Ahmad, Sens. Actuators A **167**, 60 (2011).
16. X. Li and H. Ding, Opt. Lett. **37**, 5187 (2012).
17. J. H. Chen, Y. Chen, W. Luo, J. L. Kou, F. Xu, and Y. Q. Lu, Opt. Express **22**, 17890 (2014).
18. L. Zhou, X. Sun, X. Li, and J. Chen, Sensors **11**, 6856 (2011).
19. G. Brambilla, V. Finazzi, and D. J. Richardson, Opt. Express **12**, 2258 (2004).
20. T. A. Birks and Y. W. Li, J. Lightwave Technol. **10**, 432 (1992).
21. L. Xiao and T. A. Birks, Opt. Lett. **36**, 1098 (2011).
22. X. S. Jiang, Q. Yang, G. Vienne, Y. H. Li, and L. M. Tong, Appl. Phys. Lett. **89**, 143513 (2006).
23. K. Okamoto, *Fundamentals of Optical Waveguides* (Academic, 2010).
24. J. Kou, J. Chen, Y. Chen, F. Xu, and Y. Q. Lu, Optica **1**, 307 (2014).
25. Y. Chen, F. Xu, and Y. Q. Lu, Opt. Express **19**, 22923 (2011).
26. W. Talataisong, D. N. Wang, R. Chitaree, C. R. Liao, and C. Wang, Opt. Lett. **40**, 1220 (2015).
27. D. Song, Z. Wei, J. Zou, and S. Yang, IEEE Sens. J. **9**, 828 (2009).
28. N. Tarjányi, I. Turek, and I. Martinček, Opt. Mater. **37**, 798 (2014).